

Evaluation of Operating Margin and Switching Probability of Voltage Controlled Magnetic Anisotropy (VCMA) Magnetic Tunnel Junctions

Jeehwan Song, Ibrahim Ahmed, Zhengyang Zhao, Delin Zhang, Sachin S. Sapatnekar, Jian-Ping Wang, and Chris H. Kim

Abstract—Voltage-controlled magnetic anisotropy (VCMA) has attracted great attention as it allows faster switching and lower energy consumption compared to traditional spin transfer torque (STT) based magnetization switching. In this paper, we evaluate the operating margin and switching probability of VCMA based magnetic tunnel junctions (MTJs) using realistic material and device parameters. For this study, we developed a physics-based SPICE model that incorporates various VCMA parameters such as VCMA coefficient, energy barrier, time constant, and external magnetic field. Switching probability of a VCMA device was obtained by running Monte-Carlo simulations including thermal fluctuation effects. A design space exploration was performed using the proposed simulation framework. The highest switching probabilities we were able to achieve were 94.9, 84.8, and 53.5 %, for VCMA coefficient values of 33, 105, and 290 $\text{fJ}\cdot\text{V}^{-1}\cdot\text{m}^{-1}$, respectively. Our study shows that for VCMA devices to become viable, their switching probability must be improved significantly either through new physics or material innovation.

Index Terms— Voltage-controlled magnetic anisotropy (VCMA), magnetic tunnel junction (MTJ), switching probability, VCMA coefficient.

I. INTRODUCTION

SPIN transfer torque magnetic tunnel junction (STT-MTJ) has been proven as a promising device technology for high-density non-volatile memory applications. STT phenomenon can flip the magnetization of a ferromagnetic layer using the current flowing through the tunnel barrier itself [1]–[7]. The research community has been focusing on making STT more efficient; such as reducing the write current, improving the switching time, and enhancing the tunnel magnetoresistive ratio (TMR) [7][8]. Many of these challenges stem from the fact that the current required to switch the magnetization is proportional to the energy barrier separating the two states. For example, a higher energy barrier improves the non-volatility, but requires a higher energy to flip states.

One way to alleviate this problem is to temporarily lower the energy barrier right before applying a STT current using a recently reported voltage-controlled magnetic anisotropy (VCMA) effect [9]–[12]. The amount of current needed to switch the magnetization is lower than conventional STT switching owing to the reduced energy barrier. As shown in Fig. 1, applying a positive voltage to a thick tunnel barrier MTJ device decreases the magnetic anisotropy, resulting in a lower

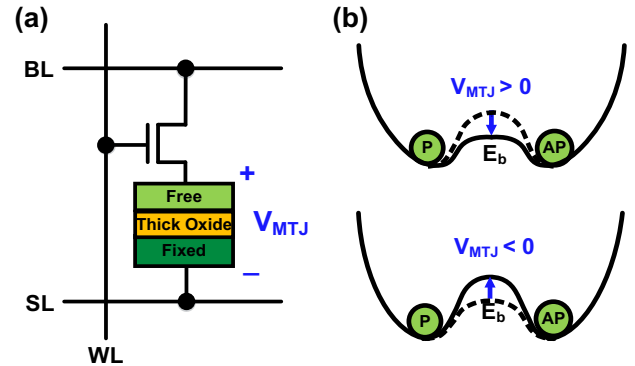


Fig. 1. (a) VCMA STT-MRAM bit cell. (b) Energy barrier of a VCMA MTJ is modulated by the applied voltage V_E . When the energy barrier is lowered, the magnetization precesses between parallel and anti-parallel states.

energy barrier. Conversely, the energy barrier is expected to increase for a negative voltage, although this has not been proven experimentally [13]. The tunnel barrier can be made thicker than a normal MTJ since the STT current required for switching is reduced by the VCMA effect. Despite the early experimental results, to our knowledge, there has not been any study on the operating margin and switching probability of VCMA devices.

In this paper, we study these critical aspects of VCMA devices and present design space exploration results. The remainder of the paper is organized as follows. Section II introduces VCMA effect and its underlying physics. Section III describes the SPICE model developed in this work. Section IV investigates the effect of material parameters and external field on the switching operation, and then switching probabilities are analyzed in Section V. Conclusions are drawn in Section VI.

II. VCMA BASICS

A. Perpendicular Magnetic Anisotropy

Depending on the direction of the easy-axis, magnetic anisotropy (MA) can be classified into perpendicular magnetic anisotropy (PMA) and in-plane magnetic anisotropy (IMA). Compared to an IMA-based device, a PMA-based device has proven to have a lower switching current for the same thermal stability factor [14]–[16]. PMA can be further classified based

its origin: interfacial PMA (iPMA) and crystalline PMA (cPMA). iPMA has been observed in CoFeB whose thickness is below the critical thickness t_c where the perpendicular anisotropy occurs, while cPMA has been observed in high crystalline anisotropy materials such as CoPt and FePd [17][18]. The effective perpendicular anisotropy field ($H_{K_{\perp}eff}$) can be expressed as

$$H_{K_{\perp}eff} = H_{K_{\perp}} - H_{dz} = 2K_{\perp}/M_s - 4\pi N_{dz}M_s \quad (1),$$

where $H_{K_{\perp}}$ is the perpendicular anisotropy field, $H_d = [H_{dx}, H_{dy}, H_{dz}]$ is the demagnetization field, M_s is the saturation magnetization, and $N_d = [N_{dx}, N_{dy}, N_{dz}]$ is the geometry-dependent demagnetization coefficient. For the interface PMA, K_{\perp} can be expressed as K_i/t_F ($= 2\pi M_s^2 t_c/t_F$) where K_i is the interfacial anisotropy energy density, and t_F is the free layer thickness. For the crystalline PMA, $K_{\perp} = K_u$ where K_u is the crystal anisotropy energy density. Since VCMA effect has traditionally been observed only in interfacial PMA material [19]-[24], we only considered iPMA-based MTJs in this study.

B. VCMA effect

Recent experiments have shown that by applying a positive voltage to an MTJ, interface PMA can be reduced [25]. The physical origin of this phenomenon is that the charge accumulation or depletion at the metal-barrier interface, which is induced by electric field, can change the magnetic anisotropy through modifying the spin-orbit interaction at the interface [26][27]. The relationship between the applied voltage and iPMA can be modeled as follows.

$$K_i = K_i|_{V=0} - \xi V/t_{ox} \quad (2),$$

where ξ is the VCMA coefficient that represents the sensitivity between MA and the applied electric field, and t_{ox} is the oxide layer thickness. The change in PMA modulates the energy barrier (E_b) of the free layer [28]. Applying a positive voltage to the oxide layer lowers the energy barrier, thus it enables the free layer's magnetization to precess between the two stable states. Compared to STT-induced switching, VCMA switching can be fast due to the lowered energy barrier, and consumes less switching energy due to the thicker tunnel barrier layer.

Thermal stability factor (TSF) of an MTJ is a critical device parameter that determines the data retention capability of a ferromagnetic layer. It is defined as the free layer's energy barrier normalized to the $k_B T$ energy [29]. VCMA induces change in K_i , which in turn changes the TSF as follows.

$$TSF = \frac{E_b}{k_B T} = \frac{(K_i - 2\pi M_s^2 t_F) A}{k_B T} \quad (3)$$

Here, E_b is the voltage-dependent energy barrier between two stable states, A is the cross-sectional area of the free-layer, k_B is the Boltzmann constant, and T is absolute temperature.

C. Thermal Fluctuation

Intrinsic randomness in the magnetization's behavior referred to as thermal fluctuation may affect the switching

characteristics. For example, it can thermally activate the magnetization's initial angle at the beginning of the writing operation, which can either induce "unwanted" switching or impede "wanted" switching [30]. To emulate the effect of thermal fluctuation in the most realistic way, random thermal field was added, not only to the initial angle, but also to the effective anisotropy field at each time step of the simulation. Since thermal field is a stochastic process, it can be modeled as a zero-mean Gaussian random distribution with a standard deviation ($\sigma_{H_{th}}$) as follows [31].

$$\sigma_{H_{th}} = \sqrt{2k_B \alpha T / (\mu_0 \gamma V_F M_s \delta t)} \quad (4)$$

Here, α is the Gilbert damping constant, μ_0 is the permeability in vacuum, γ is the gyromagnetic ratio, V_F is the volume of the free layer, and δt is the time step. A $\sigma_{H_{th}}$ value of 4.5 mT was used for all the Monte Carlo simulations in this work.

III. VCMA-MTJ SPICE MODEL SETUP

This section describes the VCMA-MTJ device model for simulating two switching schemes: VCMA only switching scheme and VCMA-assisted STT switching scheme.

A. Magnetization Dynamics

The proposed SPICE model is based on the Landau-Lifshitz-Gilbert (LLG) equation which comprises precession, damping, and spin transfer torque terms as follows.

$$\frac{1+\alpha^2}{\gamma} \cdot \frac{d\vec{M}}{dt} = -\vec{M} \times \vec{H}_{eff}(V) - \alpha \cdot \vec{M} \times (\vec{M} \times \vec{H}_{eff}(V)) + \frac{\hbar PJ}{2et_F M_s} \cdot \vec{M} \times (\vec{M} \times \vec{M}_P) \quad (5)$$

Here, \vec{M} is the magnetization vector of the free-layer, $\vec{H}_{eff}(V)$ is the voltage-dependent effective magnetic field, \hbar is the reduced Planck's constant, P is the spin polarization factor, J is the switching current density, e is the electron charge, and \vec{M}_P is the magnetization vector of fixed-layer.

More specifically, $\vec{H}_{eff}(V)$ includes different field components affecting the free layer [32].

$$\vec{H}_{eff}(V) = \vec{H}_{ext} + \vec{H}_d + \vec{H}_{th} + \vec{H}_{K_{\perp}eff}(V) \quad (6)$$

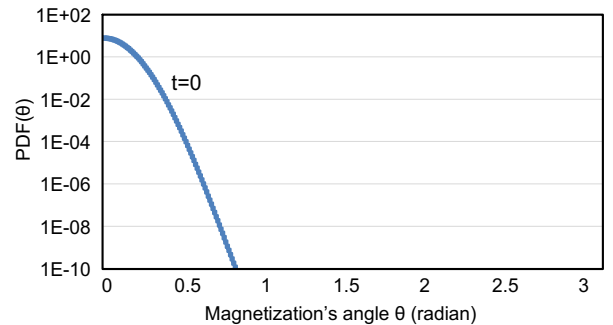


Fig. 2. Initial angle distribution, $PDF(\theta)|_{t=0}$, for TSF=45.7

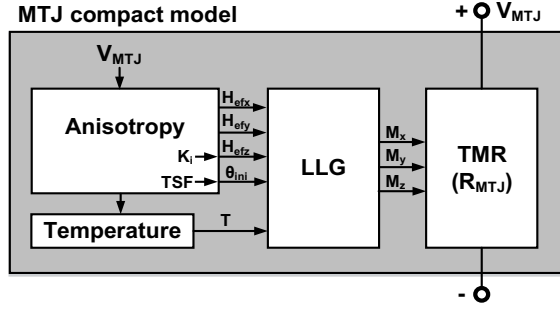


Fig. 3. Proposed VCMA based MTJ SPICE compact model.

$$\vec{H}_{K\perp eff}(V) = \left(0\vec{x}, 0\vec{y}, \left(\frac{2K_i(V)}{\mu_0 M_s t_F}\right) m_z \vec{z}\right) \quad (7)$$

Here, \vec{H}_{ext} is the external magnetic field, \vec{H}_d is the demagnetization field, \vec{H}_{th} is the thermal field, $\vec{H}_{K\perp eff}(V)$ is the voltage-dependent effective perpendicular anisotropy field, μ_0 is the permeability, $m = [m_x, m_y, m_z]$ is the magnetization moment, and $[\vec{x}, \vec{y}, \vec{z}]$ is the unit vector.

The VCMA effect can be incorporated into the LLG equation in (5) by combining (6) and (7). In addition, VCMA affects the thermal stability factor which in turn affects the \vec{M} in (5). This is because the magnetization's initial angle is a variable. It can be modeled using the Fokker-Plank distribution as below [33].

$$PDF(\theta)|_{t=0} = \frac{\exp(-TSF \cdot \sin^2 \theta)}{\int_0^\pi \sin \theta \exp(-TSF \cdot \sin^2 \theta) d\theta} \quad (8)$$

Here, $PDF(\theta)|_{t=0}$ is the initial angle's probability distribution function, TSF is the thermal stability factor, and θ is the magnetization's angle (Fig. 2).

Since we use the LLG equation and add stochasticity in the initial angle and the run-time random thermal field, our simulation method is equivalent to the stochastic LLG equation in [43].

TMR is expressed as $(R_{AP}-R_P)/R_P$ where R_{AP} and R_P are the anti-parallel and parallel resistances of the MTJ, respectively. [The voltage and temperature dependency of TMR is captured using the modified Julliere's formula as below \[44\]:](#)

$$TMR(T, V) = \frac{2P_0^2(1-\alpha_{sp}T^{3/2})^2}{1-P_0^2(1-\alpha_{sp}T^{3/2})^2} \cdot \frac{1}{1+(V/V_0)^2} \quad (9)$$

[Here, \$P_0\$ is the polarization factor, \$\alpha_{sp}\(=2e^{-5}\)\$ is the material-dependent empirical constant, and \$V_0\$ is the bias voltage where TMR is halved.](#)

The VCMA-MTJ's physical behavior can be reproduced by simulating the SPICE model shown in Fig. 3 consisting of four subcircuits: anisotropy, LLG, TMR, and temperature. Further details of the baseline LLG SPICE model can be found in [34][35].

B. Model Parameters

The simulation parameters of the VCMA-MTJ device used

TABLE I
MATERIAL PARAMETERS USED FOR SIMULATION

Symbol	Device Parameters	Values
L_X	Free Layer Width [nm]	70 ^[19]
L_Y	Free Layer Length [nm]	70 ^[19]
t_F	Free Layer Thickness [nm]	1.49
t_{OX}	Oxide Thickness [nm]	1.4 ^[19]
t_C	Critical Thickness [nm]	1.5 ^[21]
RA_P	Resistance-area Product [$\Omega \cdot \mu\text{m}^2$]	130 ^[19]
TMR_0	Tunnel Magnetoresistance @ 0V [%]	150 ^[19]
M_{S0}	Saturation Magnetization @ 0K [KA/cm]	950 ^[20]
P_0	Polarization Factor @ 0K	0.54 ^[20]
α	Damping Factor	0.025 ^[21]
ζ	VCMA Coefficient [$\text{fJ} \cdot \text{V}^{-1} \cdot \text{m}^{-1}$]	33 ^[19] , 105 ^[22] , 290 ^[23]
TSF	Thermal Stability Factor	45.7
H_{EXT}	External Magnetic Field [mT]	20 (hard-axis)
T	Temperature [K]	358

in this work are listed in Table I. For a more accurate physics-based model, device parameters are taken from state-of-the-art experimental data [19]-[23]. Three different VCMA coefficients ranging from 33 to 290 $\text{fJ} \cdot \text{V}^{-1} \cdot \text{m}^{-1}$ are considered in order to analyze its effect on the switching time and switching probability. We assume a TSF value of 45.7 [5]. To facilitate the switching, a 20mT external magnetic field was applied along the hard-axis (i.e. x-axis) [23][36][37].

C. VCMA Only Switching

When the energy barrier is lowered by the V_E voltage and external magnetic field is applied at the same time, the VCMA-MTJ's magnetization starts to oscillate around the hard-axis due to magnetization dynamics by LLG equation. By terminating the V_E pulse at the appropriate moment, the magnetization can be toggled as illustrated in Fig. 4(a). One limitation of this approach is that the switching direction is non-deterministic; i.e. we can only toggle the magnetization from its initial state. This issue can be circumvented by first reading the state of the MTJ

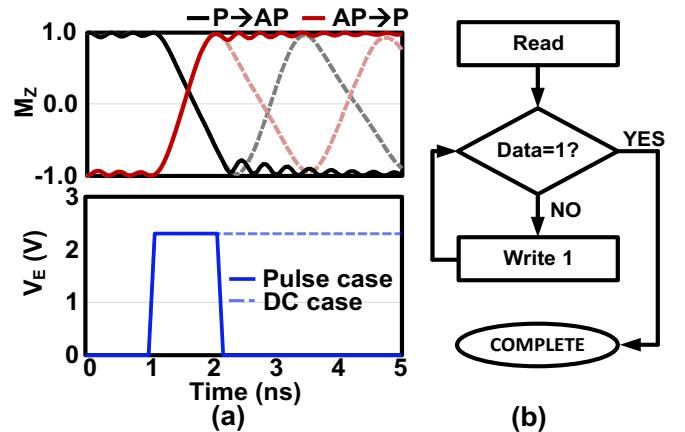


Fig. 4. VCMA only switching scheme: (a) Write voltage (V_{MTJ}) pulse and magnetization switching simulation results for VCMA device; (b) Flowchart for writing "1" into a VCMA MTJ. Due to the inherent non-deterministic switching of VCMA, a read operation is required before each write operation.

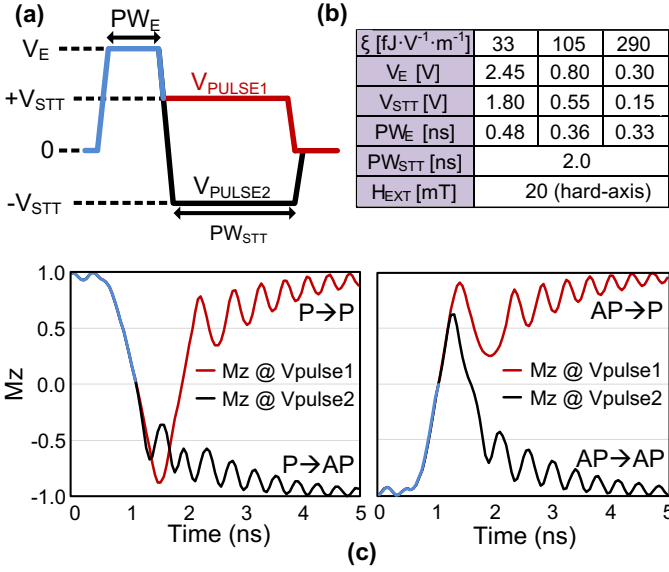


Fig. 5. VCMA-assisted STT switching scheme: (a) V_{MTJ} waveform where an initial high voltage is followed by a positive or negative STT pulse; (b) simulation parameters; (c) magnetization dynamics for P→P, P→AP, AP→P, and AP→AP switching.

and subsequently applying the write pulse as needed (Fig. 4(b)). However, this requires an additional read cycle before each write cycle.

D. VCMA-assisted STT Switching

The VCMA-assisted STT switching scheme proposed in [36] can enable deterministic switching without incurring an extra read operation. Fig. 5 shows the voltage pulse sequence where the initial V_E pulse reduces induces VCMA while the subsequent V_{STT} pulse, perfectly timed at the moment when the magnetization is near the hard-axis, tilts the magnetization to either parallel or anti-parallel state depending on the voltage polarity. In this work, we analyzed the switching characteristics of the VCMA-assisted STT switching scheme as it has the advantage of a deterministic switching state. To maximize the switching probability, we optimized the write voltage pulse (i.e. V_E , PW_E , V_{STT} , and PW_{STT} denoted in Fig. 5 (a) for each VCMA coefficient value. Fig. 5 (b) shows the optimal parameter values found through the optimization method described in Section V.

IV. MATERIAL PARAMETERS AND EXTERNAL FIELD

In this section, we present simulation results showing the impact of VCMA coefficient, response time of energy barrier, and external magnetic field on VCMA-assisted STT switching.

A. VCMA Coefficient

VCMA coefficient (ξ) is a critical parameter, which determines the sensitivity of the energy barrier to the applied electric field. It can be expressed as follows [38].

$$\xi [\text{fJ}/\text{Vm}] = \frac{\Delta \text{ Interfacial Anisotropy } [\mu\text{J}/\text{m}^2]}{\Delta \text{ Electric Field } [\text{V}/\text{nm}]} \quad (10)$$

As shown in Fig. 6, when ξ is increased from 33 to 105 $\text{fJ}\cdot\text{V}^{-1}\cdot\text{m}^{-1}$.

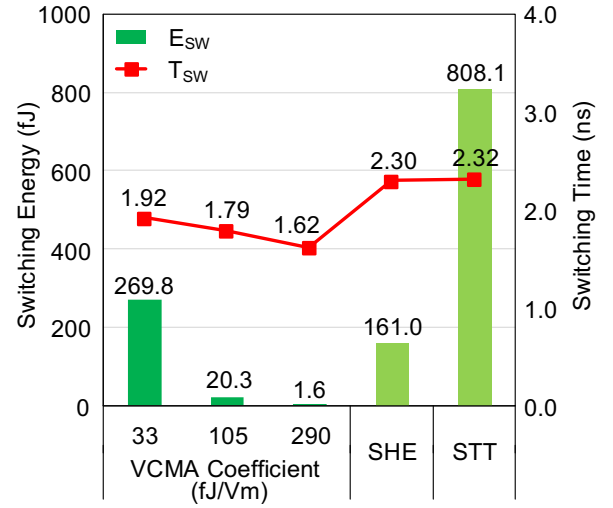


Fig. 6. Switching energy and switching time for VCMA, SHE and STT.

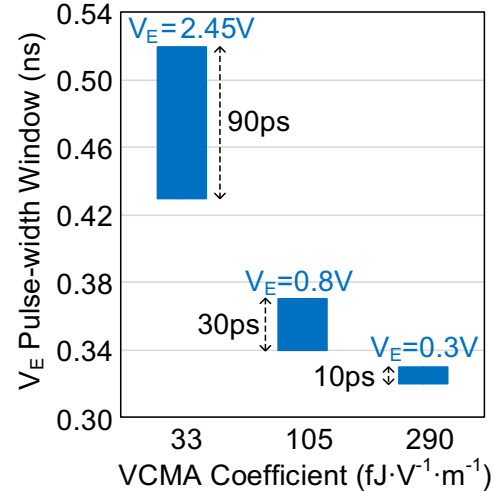


Fig. 7. Pulse width window for different VCMA coefficients.

m^{-1} , the switching time decreases by 7%. The switching time decreases further by 10% when ξ is increased from 105 to 290 $\text{fJ}\cdot\text{V}^{-1}\cdot\text{m}^{-1}$. As expected, a higher VCMA coefficient provides faster switching and lower switching energy consumption. The switching energy decreases by 13 times when ξ increases from 33 to 105 $\text{fJ}\cdot\text{V}^{-1}\cdot\text{m}^{-1}$, and by 12 times when ξ increases from 105 to 290 $\text{fJ}\cdot\text{V}^{-1}\cdot\text{m}^{-1}$. Compared to conventional STT based switching, the switching time decreases by 17%, 23%, and 30%, respectively, for $\xi=33$, 105, and 290 $\text{fJ}\cdot\text{V}^{-1}\cdot\text{m}^{-1}$. The switching energy is reduced by 3 \times , 40 \times , and 494 \times , respectively. In this comparison, we use a MTJ model with a tunneling barrier thickness of 1.0nm for conventional STT based switching [35]. In addition, compared to SHE based switching in [31], VCMA-MTJ's switching time is decreased by 17%, 22%, and 30%, respectively, for $\xi=33$, 105, and 290 $\text{fJ}\cdot\text{V}^{-1}\cdot\text{m}^{-1}$, and switching energy is reduced by 8 \times , 98 \times for $\xi=105$ and 290 $\text{fJ}\cdot\text{V}^{-1}\cdot\text{m}^{-1}$.

Recently, magnetic materials with higher VCMA coefficients have been reported [22][23][24][39]. However, as the VCMA coefficient increases, the free layer's magnetization precesses more rapidly, which makes the switching more

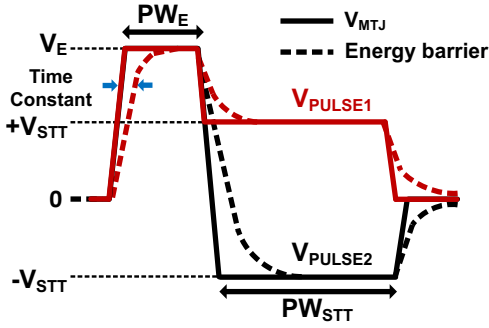


Fig. 8. Concept of time constant between applied voltage and energy barrier.

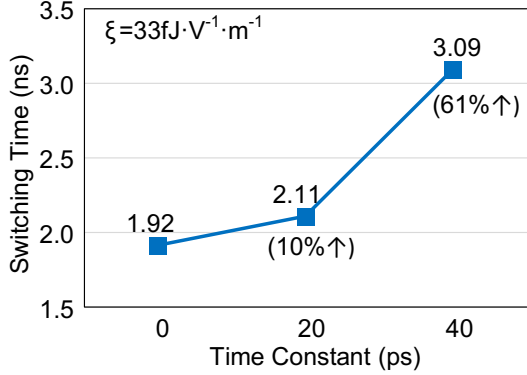


Fig. 9. Effect of energy barrier time constant on switching time.

unstable, and hence resulting in a narrower operating window. Consequently, it becomes much more difficult to capture the precise moment when the magnetization swings towards the other side of the hard-axis. This can be seen in Fig. 7 where the pulse-width window for correct switching reduces from 90ps to 10ps as the VCMA coefficient increases from 33 to 290 $\text{fJ}\cdot\text{V}^{-1}\cdot\text{m}^{-1}$. This trend suggests that extremely precise control of the voltage pulse-width (e.g. few picoseconds) is required for high VCMA coefficient materials to work reliably.

B. Response Time of Energy Barrier

We also studied the impact of response time (or time constant) between the write voltage and the free layer's energy barrier, on the switching characteristics. Fig. 8 illustrates the concept of time constant, which is the time delay between the solid line (voltage) and dashed line (energy). Since no experimental data on the energy barrier time constant exists, we simply varied the time constant and simulated the switching behavior. The time constant was implemented using a simple first-order RC delay circuit in the SPICE model. To implement the time constant effect in our simulation, the MTJ voltage is connected to a first order RC circuit before being applied to the interfacial anisotropy field in the LLG subcircuit.

As shown in Fig. 9, the switching time increased by 10% and 61%, respectively, for time constant values of 20ps and 40ps. The longer switching time can be attributed to the energy barrier not being fully removed when the V_{STT} pulse arrives. As a result, it takes longer for the magnetization to overcome the residual energy barrier, making VCMA based switching less robust.

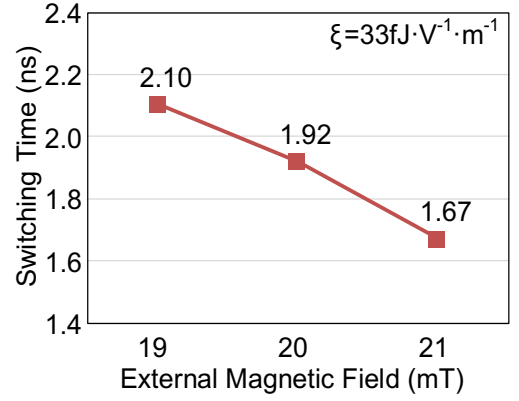


Fig. 10. Effect of external magnetic field on switching time.

C. External Magnetic Field

In order for the magnetization of a VCMA device to oscillate around the hard-axis, an external magnetic field (H_{ext}) must be applied towards this axis [25][38]. To this end, we study the effect of external magnetic field by applying different H_{ext} values and simulating the magnetization switching. As shown in Fig. 10, the switching time reduces from 2.10ns to 1.67ns as the external magnetic field is increased from 19mT to 21mT. These results indicate that a larger external magnetic field helps tilt the free layer's magnetization towards the hard-axis more quickly, which enables faster switching operation.

Applying a magnetic field using off-chip equipment is not feasible for integrated systems. Recent work has shown the feasibility of generating a local magnetic field using a composite device [40]. Here, a composite device was fabricated with an in-plane magnetic layer placed on top of a perpendicular magnetic layer. The paper shows switching of perpendicular Ta/CoFeB/MgO nanopillars in the absence of an external magnetic field. Our model assumes such a composite device where a local magnetic field is generated within each memory cell.

V. SWITCHING PROBABILITY RESULTS

A. Monte-Carlo Simulation Setup

Previous studies on VCMA-assisted STT switching have only reported results for parallel to anti-parallel (P-to-AP) and anti-parallel to parallel (AP-to-P) switching directions [19][25][36][41]. In this work, we show switching probability results for all four switching directions; i.e., P-to-AP, P-to-P, AP-to-P, and AP-to-AP. To obtain realistic results, we ran Monte-Carlo simulations using 10,000 different initial magnetization angles that were sampled from a probability density function [42]. A thermal fluctuation field of $\sigma_{H_{th}}=4.5\text{mT}$ was used as per (4).

B. Design Space Exploration

The initial simulation parameters were aimed at achieving the lowest possible energy dissipation. First, we selected the minimum V_E that allows the free layer's magnetization to oscillate around the hard-axis for both initial states. Then, the V_E pulse-width was optimized to capture the precise moment when the magnetization is set towards the hard-axis. For simplicity, the V_{STT} voltage was fixed to half the V_E voltage,

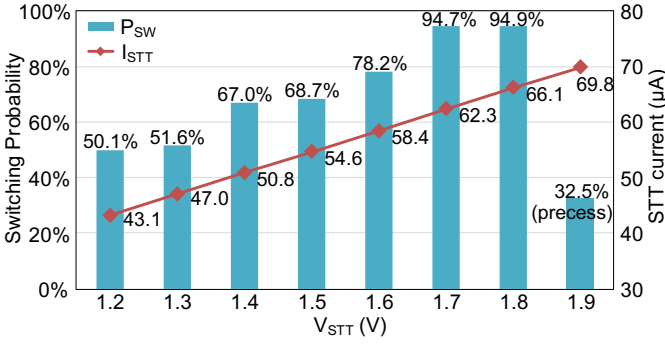


Fig. 11. Switching probability versus V_{STT} for $V_E=2.45V$.

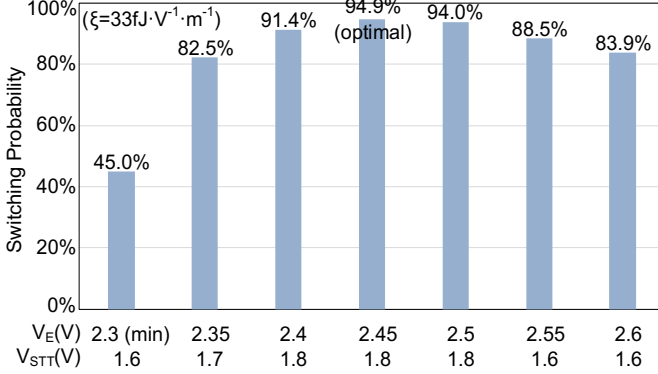


Fig. 12. Switching probability for different V_E voltages. V_E pulse-width and V_{STT} voltage were optimized for each V_E voltage.

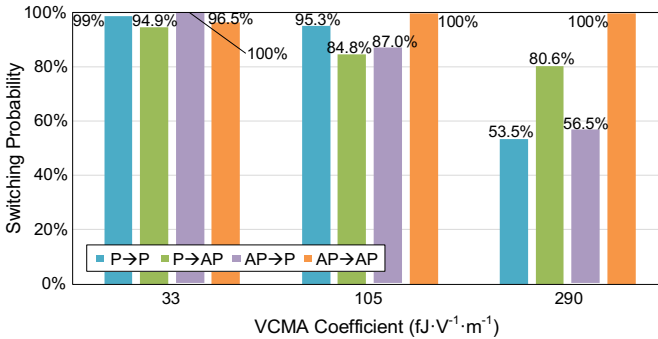


Fig. 13. Highest switching probability after optimizing V_E , V_{STT} , and pulse-width for different VCMA coefficients. Switching probabilities for all four directions are shown. Due to the unstable nature of VCMA, it is difficult to achieve switching probabilities required for practical memory applications.

and the V_{STT} pulse-width was fixed at 2.0ns. The deterministic switching probabilities using the above mentioned parameter set were in the 46%-85% range depending on the switching direction. Since these values are far too low for practical memory applications, we adjusted key design parameters such as V_E , PW_E , and V_{STT} in an attempt to improve the switching probability. Our strategy for optimizing the switching probability is summarized next.

V_{STT} amplitude: Increasing the V_{STT} voltage can induce a larger STT current, and thereby induce a stronger STT effect. This forces the magnetization to switch to the desired state, which consequently improves the switching probability. As shown in Fig. 11, the STT current increases by 53% when V_{STT} is increased from 1.2V to 1.8V, resulting in an improvement of

switching probability from 50.1% to 94.9%. However, the switching probability could not be improved further because at very high V_{STT} voltages, the magnetization has a higher chance of precessing between the two states causing unstable behavior. Therefore, increasing the V_{STT} voltage alone cannot guarantee 100% switching probability. This can be seen in Fig. 11 where the switching probability drops beyond 1.8V. Note that the optimal V_{STT} voltage was found for each individual V_E voltage. It is also worth mentioning that the spin dynamics of VCMA-assisted switching is fundamentally different from that of STT only switching. For STT only switching, the magnetization is initially aligned with the easy axis and hence STT current is responsible for the entire switching operation. For VCMA assisted switching however, STT effect is exerted when the magnetization is near the hard axis, allowing a very small STT current to induce switching.

V_E Amplitude: For our initial simulations, we chose the minimum V_E (i.e. 2.3V) required for switching because we wanted to minimize the energy consumption. However, during our rigorous simulations, we found that increasing V_E can actually reduce the energy owing to the shorter switching time. At the same time, the switching probability can be enhanced by using a higher V_E voltage. To obtain the maximum switching probability, we optimized the V_E pulse-width and V_{STT} amplitude for each V_E voltage. We considered a V_E range of 2.3V to 2.6V, and first optimized the V_E pulse-width. Next, as discussed above, the V_{STT} voltage offering the highest switching probability was found for each V_E . Fig. 12 compares the switching probability versus V_E obtained from the proposed optimization approach. The switching probability peaks at 94.9% under the condition of $V_E=2.45V$ and $V_{STT}=1.8V$. If V_E is higher than the optimal value, the V_E pulse-width becomes narrower due to faster precessional motion, resulting in a lower switching probability.

C. Effect of VCMA Coefficient on Switching Probability

Finally, the impact of VCMA coefficient on the switching probability was analyzed using Monte-Carlo simulations. In this work, we considered all four switching directions for three different VCMA coefficient cases; i.e. 33, 105, and 290 $fJ \cdot V^{-1} \cdot m^{-1}$. The V_E and V_{STT} parameters were optimized for the highest switching probability. As shown in Fig. 13 the switching probability depends on the specific switching direction. Results show that even after extensive parameter sweeping, switching probabilities for $\xi=33$, 105, and 290 $fJ \cdot V^{-1} \cdot m^{-1}$ could not reach the desired value. Moreover, the switching probability generally degrades with a higher VCMA coefficient because of the narrower operating window (see Fig. 7) which causes more errors to occur in the presence of thermal fluctuation. It's worth noting that the switching probabilities vary significantly based on the switching direction. For the highest VCMA coefficient of 290 $fJ \cdot V^{-1} \cdot m^{-1}$, the AP→AP switching was 100% correct while the P→P switching was only 53.5% correct. Despite our best efforts, we were unable to close the gap between the different switching probabilities. Our investigation shows that poor switching probability is a major concern for high VCMA coefficient material.

VI. CONCLUSION

In this work, we evaluated the switching probability of VCMA devices for a wide range of material parameters and external fields, using a SPICE compatible LLG model. Monte Carlo simulations incorporating thermal fluctuation showed a 9 times narrower operating voltage window when the VCMA coefficient increases from 33 to 290 $\text{fJ}\cdot\text{V}^{-1}\cdot\text{m}^{-1}$. This is due to the unstable switching behavior when the energy barrier becomes more sensitive to the applied voltage. We also varied the time constant between the applied voltage and the energy barrier, as well as the external magnetic field, to understand the impact on switching time. We found that the switching time increases with a longer time constant and with a lower external magnetic field. The maximum switching probabilities we were able to achieve after optimizing the voltage waveform were 94.9%, 84.8% and 53.5% for $\xi=33$, 105, and 290 $\text{fJ}\cdot\text{V}^{-1}\cdot\text{m}^{-1}$, respectively. Despite our extensive effort, the switching probability could not be improved further. This can be attributed to the inherently unstable nature of VCMA switching which relies on the delicate balance between the barrier lowering effect and STT current for a carefully timed write pulse. Even though VCMA-MTJ devices have the potential for fast switching and low switching energy, the poor switching probability issue must be addressed before they can be a viable memory device. Another possible research direction is to develop VCMA material based on fundamentally different physics that will allow more robust switching. The SPICE models and run files used in this work are available for download at mtj.umn.edu [35].

ACKNOWLEDGMENT

This work was supported in part by C-SPIN, one of the six SRC STARnet Centers, through MARCO and DARPA, and by NSF/SRC E2CDA program. The authors would like to thank the SRC industry liaisons for encouraging us to work on this topic.

REFERENCES

- [1] J.-P. Wang, S. S. Sapatnekar, C. H. Kim, *et al.*, "A Pathway to Enable Exponential Scaling for the Beyond-CMOS Era," Proceedings of the 54th Annual Design Automation Conference 2017, Vol. Part 128280, no. 16 June 2017.
- [2] S. Tehrani, B. Engel, J. M. Slaughter, *et al.*, "Recent developments in magnetic tunnel junction MRAM," IEEE Transactions on Magnetics, vol. 36, no. 5, pp. 2752-2757, Sep 2000.
- [3] J. Song, J. Kim, S. H. Kang, *et al.*, "Sensing margin trend with technology scaling in MRAM," International Journal of Circuit Theory and Applications, vol.39, no.3, pp.313-325, Mar 2011.
- [4] S. Yuasa, A. Fukushima, K. Yakushiji, *et al.*, "Future prospects of MRAM technologies," IEEE International Electron Devices Meeting (IEDM), pp.3.1.1-3.1.4, Dec 2013.
- [5] D. Apalkov, A. Khvalkovskiy, S. Watts, *et al.*, "Spin-transfer torque magnetic random access memory (STT-MRAM)," ACM Journal on Emerging Technologies in Computing Systems (JETC), vol. 9, no. 2, pp. 13:1-13:35, May 2013.
- [6] J. H. Kim, W. C. Lim, U. H. Pi, *et al.*, "Verification on the extreme scalability of STT-MRAM without loss of thermal stability below 15 nm MTJ cell," Symposium on VLSI Technology (VLSI-Technology): Digest of Technical Papers, pp. 1-2, June 2014.
- [7] E. Chen, D. Apalkov, Z. Diao, *et al.*, "Advances and Future Prospects of Spin-Transfer Torque Random Access Memory," IEEE Transactions on Magnetics, vol. 46, no. 6, pp. 1873-1878, June 2010.
- [8] K. Lee and S. H. Kang, "Development of Embedded STT-MRAM for Mobile System-on-Chips," IEEE Transactions on Magnetics, vol. 47, no. 1, pp. 131-136, Jan 2011.
- [9] M. Weisheit, S. Fähler, A. Marty, *et al.*, "Electric Field-Induced Modification of Magnetism in Thin-Film Ferromagnets," Science, vol. 315, no. 5810, pp. 349-351, Jan 2007.
- [10] T. Maruyama, Y. Shiota, T. Nozaki, *et al.*, "Large voltage-induced magnetic anisotropy change in a few atomic layers of iron," Nature Nanotechnology, vol. 4, pp. 158-161, Jan 2009.
- [11] M. Endo, S. Kanai, S. Ikeda, *et al.*, "Electric-field effects on thickness dependent magnetic anisotropy of sputtered MgO/Co40Fe40B20/Ta structures," Appl. Phys. Lett., vol. 96, no. 21, pp. 212503, May 2010.
- [12] W. G. Wang, M. Li, S. Hageman, *et al.*, "Electric-field-assisted switching in magnetic tunnel junctions," Nature Materials, vol. 11, pages 64-68, Nov 2011.
- [13] Evgeny Y. Tsymbal, "Electric toggling of magnets," Nature Materials, vol. 11, no. 1, pp. 12-13, Jan 2012.
- [14] N. Nishimura, T. Hirai, A. Koganei, *et al.*, "Magnetic tunnel junction device with perpendicular magnetization films for high-density magnetic random access memory," Journal of Applied Physics, vol 91, no. 8, pp.5246-5249, 2002.
- [15] T. Kishi, H. Yoda, T. Kai, *et al.*, "Lower-current and fast switching of a perpendicular TMR for high speed and high density spin-transfer-torque MRAM," IEEE International Electron Devices Meeting, pp.1-4, Dec 2008.
- [16] S. Peng, M. Wang, H. Yang, *et al.*, "Origin of interfacial perpendicular magnetic anisotropy in MgO/CoFe/metallic capping layer structures," Scientific Reports, vol.5, no. 18173, Dec 2015.
- [17] J. U. Thiele, L. Folks, M. F. Toney, *et al.*, "Perpendicular magnetic anisotropy and magnetic domain structure in sputtered epitaxial FePt (001) L10 films," Journal of Applied Physics, vol. 84, no. 10, pp.5686-5692, Nov 1998.
- [18] M. Ohtake, S. Ouchi, F. Kirino, *et al.*, "Structure and Magnetic Properties of CoPt, CoPd, FePt, and FePd Alloy Thin Films Formed on MgO(111) Substrates," IEEE Transactions on Magnetics, vol. 48, no. 11, pp. 3595-3598, Nov 2012.
- [19] S. Kanai, M. Yamanouchi, S. Ikeda, *et al.*, "Electric field-induced magnetization reversal in a perpendicular-anisotropy CoFeB-MgO magnetic tunnel junction," Appl. Phys. Lett., vol. 101, no. 12, pp. 122403, Sep 2012.
- [20] J. Zhu, J. A. Katine, G. E. Rowlands, *et al.*, "Voltage-Induced Ferromagnetic Resonance in Magnetic Tunnel Junctions," Phys. Rev. Lett., vol. 108, no. 19, pp. 197203, May 2012.
- [21] Y. Cui, B. Khodadadi, S. Schäfer, *et al.*, "Interfacial perpendicular magnetic anisotropy and damping parameter in ultrathin Co2FeAl films," Appl. Phys. Lett., vol. 102, no. 16, pp.162403, April 2013.
- [22] T. Nozaki, H. Arai, K. Yakushiji, *et al.*, "Magnetization switching assisted by high-frequency-voltage-induced ferromagnetic resonance," Applied Physics Express, vol. 7, no. 7, pp. 073002, June 2014.
- [23] T. Nozaki, A. Koziol-Rachwał, W. Skowroński, *et al.*, "Large Voltage-Induced Changes in the Perpendicular Magnetic Anisotropy of an MgO-Based Tunnel Junction with an Ultrathin Fe Layer," Phys. Rev. Applied, vol.5, no.4, pp.044006, April 2016.
- [24] Z. Wen, H. Sukegawa, T. Seki, *et al.*, "Voltage control of magnetic anisotropy in epitaxial Ru/Co2FeAl/MgO heterostructures," Scientific Reports, vol. 7, article no. 45026, Mar 2017.
- [25] P. K. Amiri, J. G. Alzate, X. Q. Cai, *et al.*, "Electric-Field-Controlled Magnetoelectric RAM: Progress, Challenges, and Scaling," IEEE Transactions on Magnetics, vol. 51, no. 11, pp. 3401507, Nov 2015.
- [26] C. G. Duan, J. P. Velez, R. F. Sabirianov, *et al.*, "Surface Magnetoelectric Effect in Ferromagnetic Metal Films," Phys. Rev. Lett., vol. 101, no. 13, pp. 137201, Sep 2008.
- [27] M. K. Niranjana, C. G. Duan, S. S. Jaswal, *et al.*, "Electric field effect on magnetization at the Fe/MgO(001) interface," Appl. Phys. Lett., vol. 96, pp. 222504, Jun 2010.

- [28] C. Grezes, A. Rojas Rozas, F. Ebrahimi, *et al.*, "In-plane magnetic field effect on switching voltage and thermal stability in electric-field-controlled perpendicular magnetic tunnel junctions," *AIP Advances*, vol. 6, pp. 075014, Jul 2016.
- [29] R. Heindl, A. Chaudhry, and S. E. Russek, "Estimation of thermal stability factor and intrinsic switching current from switching distributions in spin-transfer-torque devices with out-of-plane magnetic anisotropy," *AIP Advances*, vol. 8, no. 1, pp. 015011, Jan 2018.
- [30] K. Munira, W. H. Butler, and A. W. Ghosh, "A Quasi-Analytical Model for Energy-Delay-Reliability Tradeoff Studies During Write Operations in a Perpendicular STT-RAM Cell," *IEEE Transactions on Electron Devices*, vol. 59, no. 8, pp. 221-2226, Aug 2012.
- [31] I. Ahmed, Z. Zhao, M. G. Mankalale, *et al.*, "A Comparative Study Between Spin-Transfer-Torque and Spin-Hall-Effect Switching Mechanisms in PMTJ Using SPICE," *IEEE Journal on Exploratory Solid-State Computational Devices and Circuits*, vol. 3, pp. 74-82, Oct 2017.
- [32] W. Kang, Y. Ran, Y. Zhang, *et al.*, "Modeling and Exploration of the Voltage-Controlled Magnetic Anisotropy Effect for the Next-generation Low-Power and High-Speed MRAM Applications," *IEEE Transactions on Nanotechnology*, vol. 16, no. 3, pp. 387-395, May 2017.
- [33] W. H. Butler, T. Mewes, C. K. A. Mewes, *et al.*, "Switching distributions for perpendicular spin-torque devices within the macrospin approximation," *IEEE Trans. Magn.*, vol. 48, no. 12, pp. 4684-4700, Dec. 2012.
- [34] J. Kim, A. Chen, B. Behin-Aein, *et al.*, "A technology-agnostic MTJ SPICE model with user-defined dimensions for STT-MRAM scalability studies," *Custom Integrated Circuits Conference (CICC)*, 2015 IEEE Date of Conference, pp. 1-4, Sep 2015.
- [35] UMN MTJ SPICE model. [Online]. Available: <http://mtj.umn.edu>
- [36] S. Kanai, Y. Nakatani, M. Yamanouchi, *et al.*, "Magnetization switching in a CoFeB/MgO magnetic tunnel junction by combining spin-transfer torque and electric field-effect," *Appl. Phys. Lett.*, vol. 104, no. 21, pp. 212406, May 2014.
- [37] A. Sengupta, A. Jaiswal, and K. Roy, "True Random Number Generation Using Voltage Controlled Spin-Dice," *Device Research Conference (DRC)*, Jun 2016.
- [38] J. G. A. Vinasco, "Voltage-Controlled Magnetic Dynamics in Nanoscale Magnetic Tunnel Junctions," Ph.D. dissertation, Dept. Elect. Eng., University of California Los Angeles, Los Angeles, CA, 2014.
- [39] A. Koziol-Rachwał, T. Nozaki, K. Freindl, *et al.*, "Enhancement of perpendicular magnetic anisotropy and its electric field-induced change through interface engineering in Cr/Fe/MgO," *Scientific Reports*, vol. 7, article no. 5993, July 2017.
- [40] Z. Zhao, A. K. Smith, M. Jamali, *et al.*, "External-Field-Free Spin Hall Switching of Perpendicular Magnetic Nanopillar with a Dipole-Coupled Composite Structure," Oct 2017, [Online]. Available: <https://arxiv.org/abs/1603.09624>
- [41] S. Sharmin, A. Jaiswal, and K. Roy, "Modeling and Design Space Exploration for Bit-Cells Based on Voltage-Assisted Switching of Magnetic Tunnel Junctions," *IEEE Transactions on Electron Devices*, vol. 63, no. 9 pp. 3493-3500, Sep 2016.
- [42] N. Kani, S. Rakheja, and A. Naeemi, "A Probability-Density Function Approach to Capture the Stochastic Dynamics of the Nanomagnet and Impact on Circuit Performance," *IEEE Transactions on Electron Devices*, vol. 63, no. 10, Oct 2016.
- [43] M. H. Jin, B. Zheng, L. Xiong, *et al.*, "Numerical simulations of critical dynamics in anisotropic magnetic films with the stochastic Landau-Lifshitz-Gilbert equation", *Physical Review E*, vol. 98, no. 2, Aug 2018
- [44] [A. Vatankhahghadam, S. Huda, A. Sheikholeslami, "A Survey on Circuit Modeling of Spin-Transfer-Torque Magnetic Tunnel Junctions", *IEEE Transactions on Circuits and Systems I: Regular Papers*, vol. 61, no. 9, pp. 2634 - 2643, Sep 2014](#)



Jeehwan Song received his B.E. degree in radio communications engineering from Korea University, Seoul, South Korea, in 2007, and M.S. degree in electrical and electronic engineering from Yonsei University, Seoul, South Korea, in 2009. He is currently pursuing a Ph.D. degree in electrical engineering at the University of Minnesota, Minneapolis, MN. His current research focuses mixed-signal circuit design for spin-based memories.



Ibrahim Ahmed is currently pursuing Ph.D. degree in Electrical Engineering at the University of Minnesota, Twin Cities, Minnesota. He received B.Sc. in Electrical and Electronic Engineering from Bangladesh University of Engineering and Technology (BUET), Dhaka, Bangladesh in 2013. His research focuses on design beyond CMOS devices and architectures, and modeling of spin based memories.



Zhengyang Zhao is currently pursuing the Ph.D. degree in Electrical Engineering at the University of Minnesota, Minneapolis, MN. He received the B.S. degree in Electrical Engineering from Xi'an Jiaotong University, China, in 2012. His research focuses on development of novel spintronic devices for energy-efficient logic and memories.



Delin Zhang received his Ph.D. degree from University of Science and Technology Beijing, China in 2012. In 2012, he joined Max Planck Institute for Chemical Physics of Solids, Dresden, Germany as a post-doctoral scientist. He has been a post-doctoral in Electrical and Computer Engineering at the University of Minnesota, Minneapolis, MN from 2014. His research focuses on exploring new perpendicular magnetic anisotropy materials, and developing high-performance spintronic logic and memories.



Sachin S. Sapatnekar is the Henle Chair in ECE and the Distinguished McKnight University Professorship at the University of Minnesota. He received his PhD from the University of Illinois at Urbana-Champaign in 1992. He is a recipient of the NSF Career Award, seven Best Paper awards, the ICCAD Ten Year Retrospective Most Influential Paper Award, the SRC Technical Excellence award, and the SIA University Research Award.



Jian Ping Wang is the Robert Hartman Chair and a Distinguished McKnight University Professor of Electrical and Computer Engineering, and a member of the graduate faculty in Physics and Chemical Engineering at the University of Minnesota. He was the director of the Center for Spintronic Materials, Novel Interfaces and Architectures (CSPIN). His current research focuses on searching, fabricating and fundamentally understanding new nanomagnetic and spintronic materials and devices.



Chris H. Kim (M'04, SM'10) received his B.S. and M.S. degrees from Seoul National University and a Ph.D. degree from Purdue University. He is currently a professor at the University of Minnesota. He is the recipient of the Taylor Award for Distinguished Research, SRC Technical Excellence Award, NSF CAREER Award, DAC/ISSCC Student Design Contest Awards, and IEEE Circuits and Systems Society Outstanding Young Author Award.